processes

MDPI

Article

Preliminary Study on Size Effect of Fractured Rock Mass with Sand Powder 3D Printing

Wenhai Wang [1], Yang Zhao [1,*], Lishuai Jiang [1,2,*], Jiacheng Zuo [1], Guangsheng Liu [3] and Hani S. Mitri [4]

[1] College of Energy and Mining Engineering, Shandong University of Science and Technology, Qingdao 266590, China
[2] State Key Laboratory of Mining Response and Disaster Prevention and Control in Deep Coal Mines, Anhui University of Science and Technology, Huainan 232001, China
[3] BGRIMM Technology Group, Beijing 100160, China
[4] Department of Mining and Materials Engineering, McGill University, Montreal, QC H3A0E8, Canada
* Correspondence: mrzhao_y@163.com (Y.Z.); lsjiang@sdust.edu.cn (L.J.)

Abstract: The size effect has a significant effect on the mechanical behavior of rock, thereby fundamentally influencing the stability of rock excavations. The main challenge associated with the experimental research on the size effect of fractured rock mass lies in the difficulty of specimen preparation to represent the influence of size and fracture on the mechanical behavior of the rock material. In order to preliminarily explore the feasibility of 3D printing technology in the field of rock mechanics, fractured rock specimens of different sizes and different fracture characteristics were produced using sand powder 3D printing technology. The uniaxial compression test was combined with the digital image correlation method (DIC) technology to study the influence of the size effect on the mechanical properties and deformation and failure of different fractured specimens. The research finds that: (1) The elastoplastic mechanical characteristics of the sand powder 3D printed specimens are similar to soft rock. Specimen size and fracture angle have significant effects on the mechanical properties of specimens. Under different fracture conditions, the uniaxial compressive strength (UCS) and Elasticity Modulus of sand powder 3D specimens should be decreased with the increase of the specimen size, and the size effect has different influences on the specimens with different fracture characteristics. (2) Under different fracture conditions, the crack initiation position and failure mode of specimens of various sizes are affected by the fracture inclination to varying degrees. (3) The size effect of fractured rock mass is closely related to the defect level inside the rock mass. The size effect originates from the heterogeneity inside the material. The research results verify the feasibility of applying sand powder 3D printing technology to study the size effect of fractured rock masses and provide an innovative test method for the size effect test study. Preliminary exploration of the size effect of fractured rock masses provides a powerful reference for related research in this field. The study proves the feasibility of applying sand powder 3D printing technology in similar rock mechanics tests and contributes to understanding the size effect of a fractured rock mass.

Keywords: size effect; sand powder 3D printing; fractured rock mass; mechanical properties; failure characteristics; mechanism analysis

Citation: Wang, W.; Zhao, Y.; Jiang, L.; Zuo, J.; Liu, G.; Mitri, H.S. Preliminary Study on Size Effect of Fractured Rock Mass with Sand Powder 3D Printing. *Processes* **2022**, *10*, 1974. https://doi.org/10.3390/pr10101974

Academic Editor: Yong Yuan

Received: 2 September 2022
Accepted: 25 September 2022
Published: 30 September 2022

1. Introduction

As a natural geological material, rock contains defects such as fractures and joints and has strong heterogeneity, which leads to certain differences in the strength and deformation characteristics of different size rocks, that is, a size effect [1,2]. Because the mechanical properties and parameters of rock mass are the important basis of surrounding rock stability analysis, support design analysis, and calculation. Therefore, the rock size effect has been one of the hot issues in rock mechanics for a long time [3,4].

Scholars have carried out a large number of experimental studies on the rock size effect. Weibull [5] proposed the strength theory of rock-like materials based on statistical

theory and believed that the ultimate strength of rock-like materials could be determined by the integral of its volume and the statistical distribution function. Bazant [6] studied and analyzed the size effect with the help of fracture mechanics and elaborated on the influence of the size effect on the strength of brittle materials from the theoretical perspective. Li et al. [7] studied the size effect of slate specimens with different bedding inclinations and analyzed the relationship between compressive strength, specimen size, foliation orientation, and confining pressure. Zhai et al. [8] conducted mechanical experiments on two soft rocks (limestone and artificial rock), respectively, studied the influence of size effect on their mechanical parameters, and proposed a suitable model for them. Faramarzi and Rezaee [9] investigated the effects of grain size and specimen size on the mechanical properties of cementitious material and presented the SEL-I model to predict specimen strength.

To sum up, scholars at home and abroad have made many achievements in this field [5–9]. However, the following questions about the rock size effect remain to be further explored: (1) at present, the size effect research is mainly aimed at the complete rock specimen [10,11], and less studied is the size effect of fractured specimens. Coal mine surrounding rock is affected by sedimentation, resulting in weak strength and the development of joints and fractures [12–15]. These weak structures have a significant impact on the mechanical properties of the rock mass and the surrounding rock stability. It is necessary to deeply study the influence of mechanical properties, deformation, and failure characteristics of fractured rock mass with the specimen size, that is, the size effect of the rock mass. (2) Natural rock has high heterogeneity [1,9]. At the same time, restricted by the sampling environment, sampling equipment, and other conditions, the test results of rock specimens are highly discrete, which affects the test results' accuracy and reliability. (3) The size effect experiment requires different volumes of specimens. The larger size specimens have many problems, such as difficult processing, high equipment requirements, and difficulty in testing. Therefore, many scholars use theoretical analysis or numerical simulation methods to study the rock size effect [16–18].

Three-dimensional (3D) printing technology has developed rapidly in recent years. Various kinds of specimens with complex structures can be accurately produced, which breaks through the limitations of traditional methods in the preparation of complex fracture specimens [19–21]. It provides a new method for experimental research of rock mechanics, especially in fractured rock mechanics. Ju et al. [19] used CT scan, 3D reconstruction, and 3D printing technology to produce a physical model representing the natural coal rock and study the influences of discontinuous, irregular fractures on the strength, deformation, and stress concentration of coal rock. Jiang et al. [20] conducted a uniaxial test and a triaxial compression test on the 3D printed specimens, proving that their mechanical properties and failure patterns are similar to natural rocks. Kong et al. [21] studied the mechanical properties of 3D-printed gypsum specimens through uniaxial compression tests, proving the feasibility and reliability of 3D printing technology. It can be seen that 3D printing technology has attracted the extensive attention of many scholars at home and abroad. The feasibility in the field of rock mechanics has been fully confirmed and affirmed, indicating that it has broad research and application prospects.

Sand powder 3D printing technology based on the powder bonding molding process has emerged since 2017 [22]. It is a three-dimensional model construction technology that uses a sand powder 3D printer to spray the powder material according to the cross-sectional data of the test specimen and then forms a molding entity by bonding into layers and stacking layer by layer. The printing method for specimens is considered to be similar to the natural deposition of sand to form sandstone, which has attracted extensive attention from scholars in the field of rock at home and abroad [22–25]. Tian and Han [22] applied 3DP technology to prepare solid specimens simulating rock-type materials combined with computed tomography scanning and 3D image processing, and it provided technology that provided a new perspective for conducting experimental laboratory research on rock mechanics. Gomez et al. [23] investigated the suitability of using reservoir sandstone analogs, 3D printed with silica sand, to analyze the behavior of natural rocks. The 3D-

printed sandstone analogs were found to be more compressible and permeable. Xu and Jiang [24] studied the effect of printing layer thickness on the mechanical properties of sand powder 3D printing specimens and obtained specimens whose strength and other properties were closer to those of rocks by optimizing printing parameters. Through uniaxial compression and Hopkinson pressure bar experiment on sand powder 3D printing specimens, Jiang et al. [25] revealed the similarities between the mechanical properties of sand powder 3D printing specimens and soft rock in terms of static and dynamic properties. To sum up, the latest research of domestic and foreign scholars shows that the strength of sand powder 3D printed specimens is slightly lower than that of natural rocks, the uniaxial compressive strength is 5–16 MPa, and the elastoplastic mechanical performance of sand powder 3D printed specimens is similar to soft rocks such as coal and mudstone [1,26], showing typical brittle failure characteristics after peak stress. Therefore, it is considered by many scholars at home and abroad as an ideal printing substrate for simulating soft rock.

The size effect is a well-known and important effect in the fracture study of rocks. As a long-lasting research topic, the physical tests of size effect have attracted lots of research attempts and obtained lots of useful results. However, the physical tests on the size effect of fractured rock are limited by the following aspects: (1) preparation of real rock/rock-like specimens in different sizes; (2) generation of fractures in specimens. With the help of 3D printing, these two bottle-neck problems can be overcome, and thereby a novel method for creating rock-like specimens with designed fractures of any size. To validate such a methodology, it is essential to carry out preliminary experimental research to see whether this method can simulate the mechanical behaviors of rocks.

Therefore, in this study, the sand powder 3D printing technology suitable for simulating the mechanical properties of soft rock in coal measure strata is adopted, the fractured specimens with different sizes and different fracture characteristics were made, and the influence of size effect on the mechanical properties and deformation failure of different size specimens corresponding to different fracture angle was studied by combining uniaxial compression test with digital image correlation (DIC) technology. The research results verify the feasibility of applying sand powder 3D printing technology to study the size effect of fractured rock mass and provide an innovative test method for the study of size effect.

The significance of this study to the fields and industries of rock engineering, e.g., the tunneling, underground space, and mining industries. Firstly, the feasibility of applying sand powder 3D printing in similar rock mechanics tests has been proved. Secondly, the results of this study contribute to understanding the size effects of fractured rock mass and hereby improve the stability and support design of fractured rock engineering.

2. Preparation and Experimental Design of Sand Powder 3D Printing Fractured Specimens

2.1. Preparation of Sand Powder 3D Printing Specimen

According to the molding process, 3D printing technology includes Fused Deposition Modeling (FDM), Binder Jetting Technology (BJT), Selective Laser Sintering(SLS), etc. [27–29]. On the basis of previous research, considering the mechanical characteristics of coal-measure formation rocks, the BJT was selected for the preparation of specimens. The 3D printer model was VX1000 (Figure 1), was produced by Voxeljet China Co. Ltd.(Suzhou, China) the resolution is up to 600 dpi, and the maximum volume of an object that can be constructed is 0.3 m^3, GS19 sand powder, and Furan Resin were used as printing material and a binder respectively, produced by Voxeljet China Co. Ltd. The specimen preparation process was as follows. First of all, the specimen graphics were drawn by 3-dimensional software, and processing code files were generated through software and imported into the printer through a computer. Then, the printer nozzle sprayed the binder on the powder layer of the forming cylinder according to the cross-sectional shape. The forming cylinder was correspondingly lowered by 1 layer of printing height, and the powder feeding cylinder was raised one layer of printing height accordingly after 1 layer; the printer printed layers from bottom to top. Finally, the printed specimen was obtained according to the digital model; the printing principle of BJT is shown in Figure 2. When the

sand powder 3D printer prints the location of the prefabricated fracture within each layer, the powder feeding roller delivers powder, but the printer nozzle does not spray the binder. The sand powder is sealed inside the specimen and can be removed after fully bonded.

Figure 1. VX1000 3D printer.

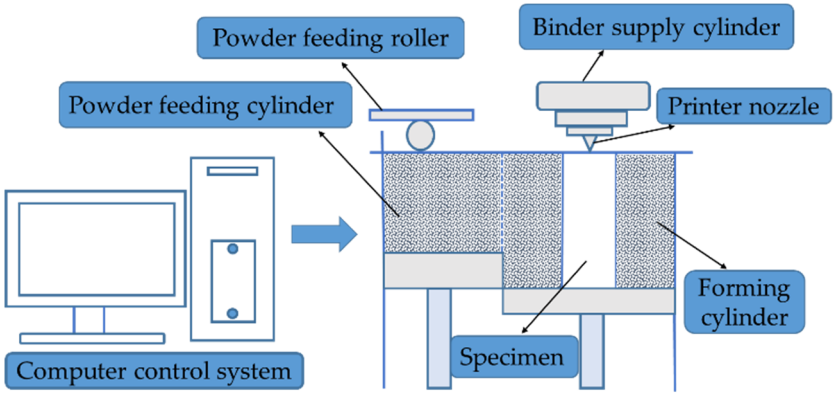

Figure 2. BJT printing principle.

The uniaxial compression test, triaxial compression test, and indirect tension test, etc., were carried out on sand powder 3D printing specimens and natural coal specimens, and the mechanical parameters such as compressive strength, tensile strength, and internal friction angle, etc., were measured. Test results are shown in Table 1 [25,30]. The overall mechanical properties of sand powder 3D printing specimens are similar to those of coal specimens, which can be used to make coal-like specimens to simulate soft rock in coal measure strata.

Table 1. Mechanical parameters of 3D printing specimen and coal specimen [25,30].

Specimen ID	Compressive Strength (MPa)	Tensile Strength (MPa)	Internal Friction Angle (°)	Cohesive Strength (MPa)	Elastic Modulus (GPa)
SLS printed specimens	3.45	0.53	47.19	0.49	1.38
BJT printed specimens	8.46	0.53	30.79	1.15	0.96
natural coal specimens	10.61	0.72	31.00	1.40	1.17

2.2. Experimental Design

The specific parameters of the specimen type in this experiment are shown in Table 2. The length-to-diameter ratio of the specimen was fixed at 2:1. The fracture length and fracture width should be multiplied with the increase in specimen volume. The appearance of the 3D printing experiment specimens is shown in Figure 3. In order to facilitate the processing of experiment results and the specimens are numbered, "L-50", "L-75," and "L-100" are used to represent specimens with sizes of 50 × 50 × 100 mm, 75 × 75 × 150 mm, and 100 × 100 × 200 mm. The fracture angles of each size specimen include 0°, 30°, 60°, and 90°.

Table 2. Specimen type parameter.

Specimen Number	Specimen Size (mm)	Fracture Length (mm)	Fracture Width (mm)	Fracture Angle (°)
L-50	50 × 50 × 100 mm	15	1.5	0°, 30°, 60°, 90°
L-75	75 × 75 × 150 mm	22.5	2.25	
L-100	100 × 100 × 200 mm	30	3.0	

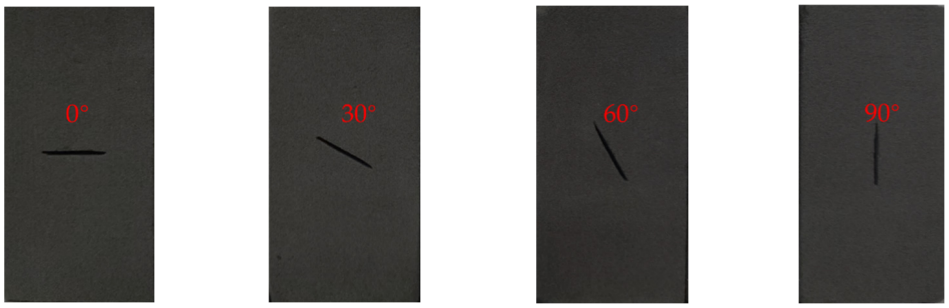

(**a**) 0° fracture angle (**b**) 30° fracture angle (**c**) 60° fracture angle (**d**) 90° fracture angle

Figure 3. 3D printing experiment specimens with different inclination angles.

The uniaxial compression test was combined with Digital Image Correlation Method (DIC) technology, which consists of loading equipment, image acquisition equipment, and light-filling equipment (Figure 4). The loading equipment was an RLJW-2000 rock rheometer with a maximum loading capacity of 800 KN. It was produced in China, and the displacement, stress, and other data can be recorded at the same time. The uniaxial compression tests were conducted according to the standard for mechanical properties on rock (DZ/T 0276.18-2015, DZ/T 0276.19-2015, China) [31,32]. The loading mode was displacement control with a loading rate of 0.001 mm/s. The displacement control should be compared with the load-control loading method; it has higher accuracy and can obtain a complete strain-strain curve. The compression process used an industrial camera to capture digital images at a rate of 1 frame/s. The industrial camera model is DMK 33UX183, designed by Germany. The light-filling equipment was placed next to the industrial camera to ensure that the image collected was clear enough. The uniaxial compression test was performed with DIC at the same time.

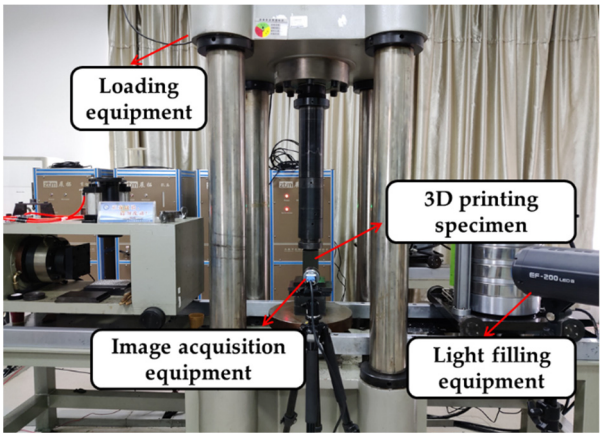

Figure 4. The test system.

3. Analysis of the Size Effect of Fractured Specimens

3.1. Analysis of Influence of Fractured Specimen Size on Uniaxial Compression Strength (UCS)

For each design of specimen, three identical specimens are prepared and tested. Due to the length of the article, one typical stress-strain curve and DIC result for each group were chosen for detailed analysis in the following section. The mechanical and deformation parameters of the specimen were calculated according to the relevant standards [31,32]. The stress-strain curves obtained from uniaxial compression tests on specimens with different sizes corresponding to different fracture angles are shown in Figure 5. It can be seen that size and fracture angle have a significant influence on the mechanical properties of the specimen. The stress-strain curves of all kinds of specimens show the microfracture closure stage (OA), the elastic stage (AB), the plastic deformation stage (BC), and the post-peak brittle failure stage (CD), and the elastic-plastic mechanical characteristics are similar to those of soft rock [20]. As shown in Figure 5d, when the fracture angle α is 90°, the UCS of L-50 is 7.39 MPa. With the increase in specimen size, the UCS of L-75 and L-100 decreases to 5.96 MPa and 5.41MPa, which decrease by 19% and 27%, respectively, and the size effect of specimen strength is significant. Figure 6 shows the influence of specimen size on the UCS with different fractured specimens. The UCS of each fractured specimen decreases with the increase of size; the size effect of 0° fractured specimens is the most significant among them. The UCS of the L-50 specimen is 5.18 MPa, and L-75 and L-100 decreased to 3.95 MPa and 3.53 MPa, 24% and 32%, respectively. However, the size effect of 30° fractured specimens is the least significant; the UCS of L-75 and L-100 decreased by 11% and 15% with the increase in specimen size, respectively. In conclusion, the size effect of 3D printing fractured specimen UCS is significant and different. It should be noted that most previous research on rock size effects is conducted with intact rock or rock-like specimens. In comparison to these studies, the presented UCS results and the obtained patterns, conducted with fractured specimens, show good agreement [8,9].

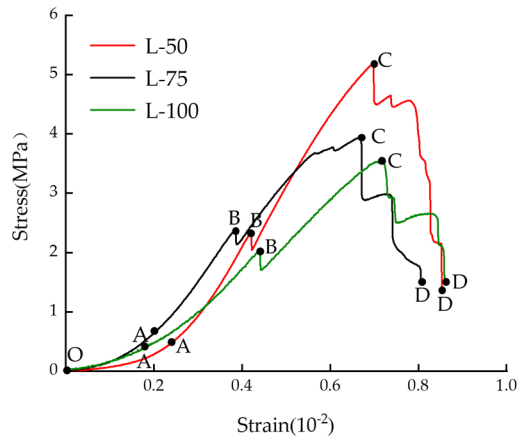

(**a**) Stress−strain curve of 0° fractured specimen

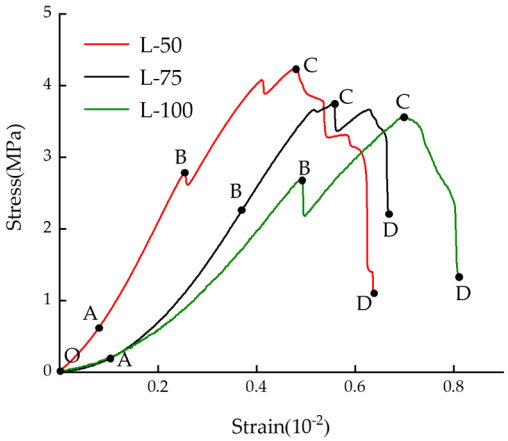

(**b**) Stress−strain curve of 30° fractured specimen

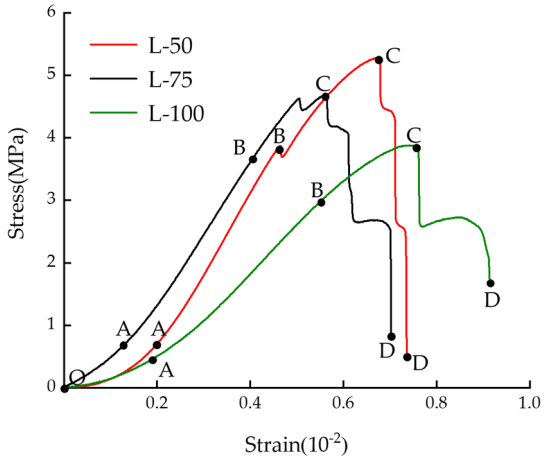

(**c**) Stress−-strain curve of 60° fractured specimen

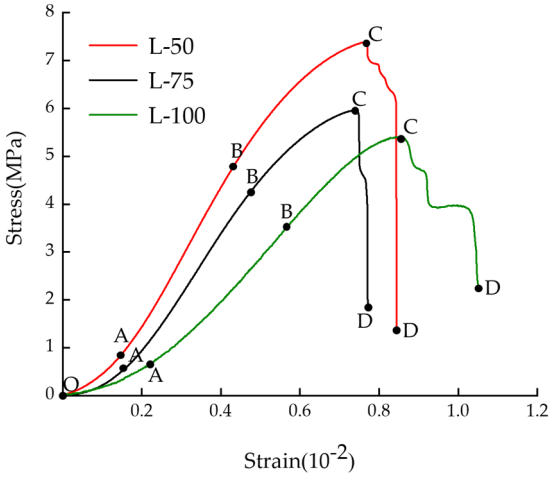

(**d**) Stress−-strain curve of 90° fractured specimen

Figure 5. The stress−strain curves of fractured specimens.

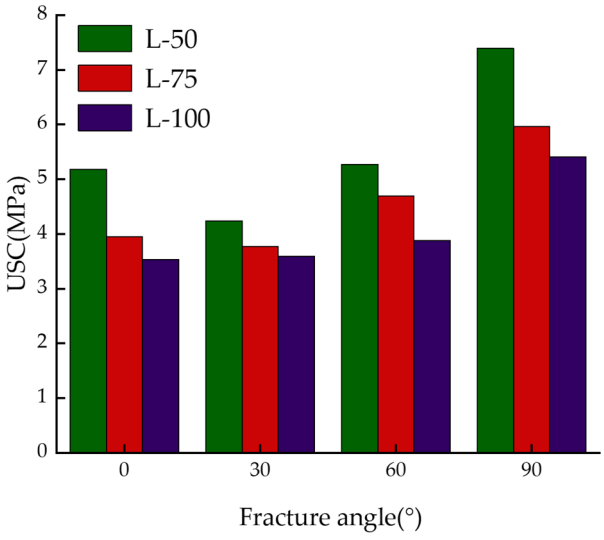

Figure 6. The relationship between size and UCS under the same fracture condition.

3.2. Analysis of Influence of Fractured Specimen Size on Elasticity Modulus

Elasticity modulus can be used to reflect the elastic stage stiffness of rock and represents the capacity of a rock to resist elastic deformation [1]. The influence of the size effect on the Elasticity Modulus with different fractured specimens is shown in Figure 7. It can be seen that the size effect of the fractured rock mass has a significant influence on the Elasticity Modulus. The Elasticity Modulus of each fractured specimen decreases with the increase of specimen size. When the specimen size range was L-50~L-75, the change of the 30° fractured specimen was the most obvious. L-50 is 1.32 GPa, L-75 decreased by 22% to 1.03 GPa. However, the change in the 60° fractured specimen was the least obvious, which only decreased by 11%. When the specimen size range is L-75~L-100, the change of the 60° fractured specimen was the most obvious. L-75 is 1.17 GPa, L-100 decreases 33% to 0.78 GPa. However, the change in the 30° fractured specimen was the least obvious, which only decreased by 20%. In conclusion, the size effect has different effects on the Elasticity Modulus of specimens with different fracture characteristics, among which 30° and 60° fracture specimens in different size ranges are the most significant. It is a well-known fact that the existence of a fracture directly affects the elasticity modulus of specimens. However, due to the difficulties in the preparation of fractured specimens, previous studies on the size effect were mainly conducted with intact or relatively small specimens [33]. Therefore, the results in UCS have been validated by comparing them with previous studies, as described in Section 3.1, which serve to validate the presented experiments and results.

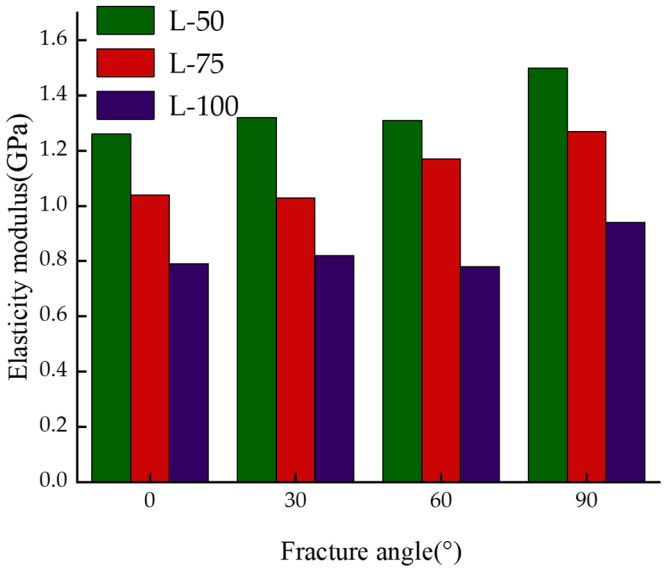

Figure 7. The relationship between size and elasticity modulus under the same fracture condition.

3.3. Analysis of Crack Evolution Process of Fractured Specimen

Figures 8–11 depict the global strain field evolution diagrams of the different fractured specimens after processing by the digital speckle system; it corresponds to each characteristic stage of the stress-strain curve (the elastic stage, the plastic deformation stage, and the post-peak brittle failure stage). Taking the stress at each stage as the axis, through the evolution rule of the global strain field and the strain concentration band, the crack evolution rule of the fractured specimen is analyzed. The ε1 represents the principal strain, and the Lagrange represents the strain in the form of the Lagrange finite strain in the figure.

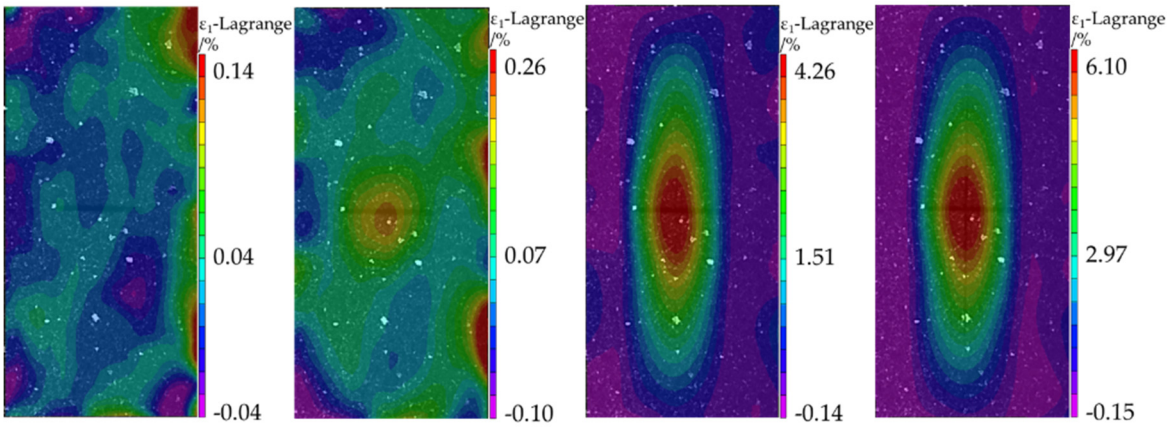

1.04 MPa 1.87 MPa 5.18 MPa (UCS) post-peak stage

(**a**) L-50

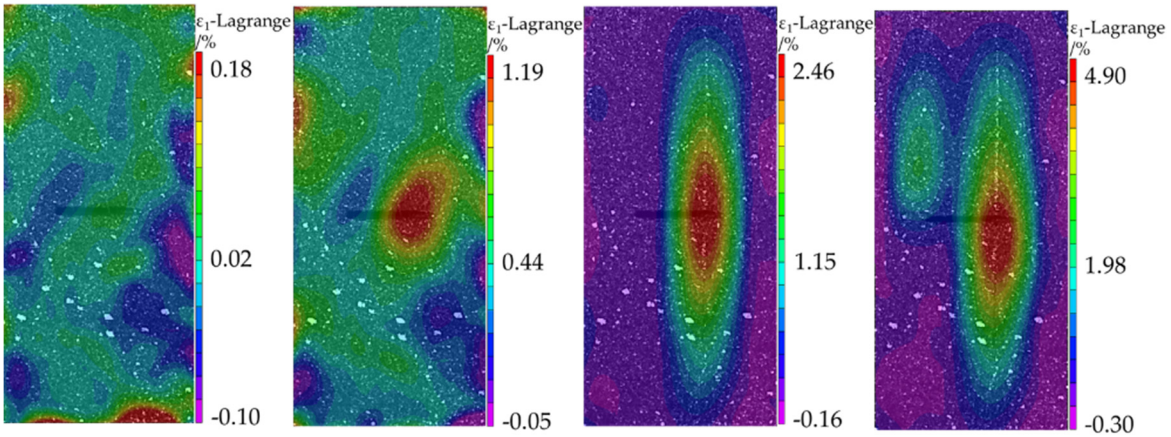

1.02 MPa 2.18 MPa 3.95 MPa (UCS) post-peak stage

(**b**) L-75

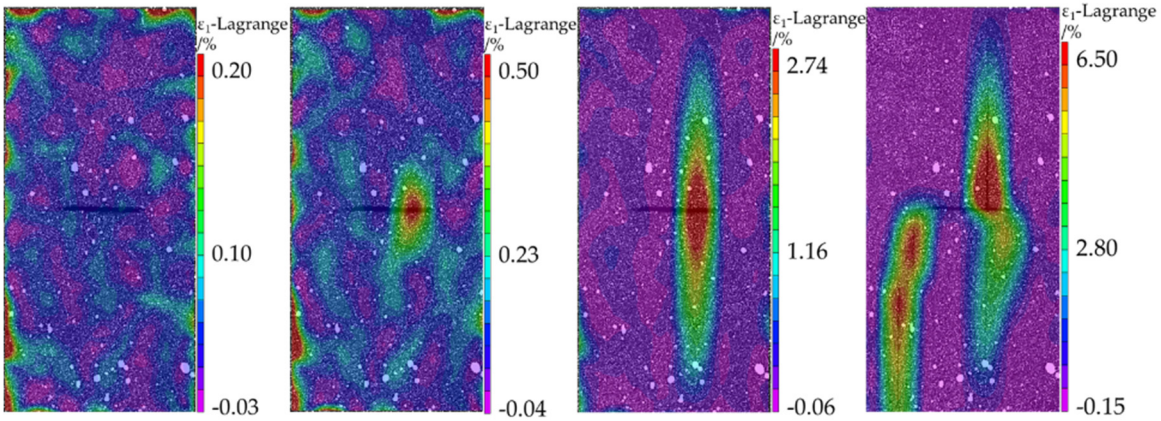

1.21 MPa 2.16 MPa 3.53 MPa (UCS) post-peak stage

(**c**) L-100

Figure 8. Evolution of the global strain field of the 0° fractured specimen.

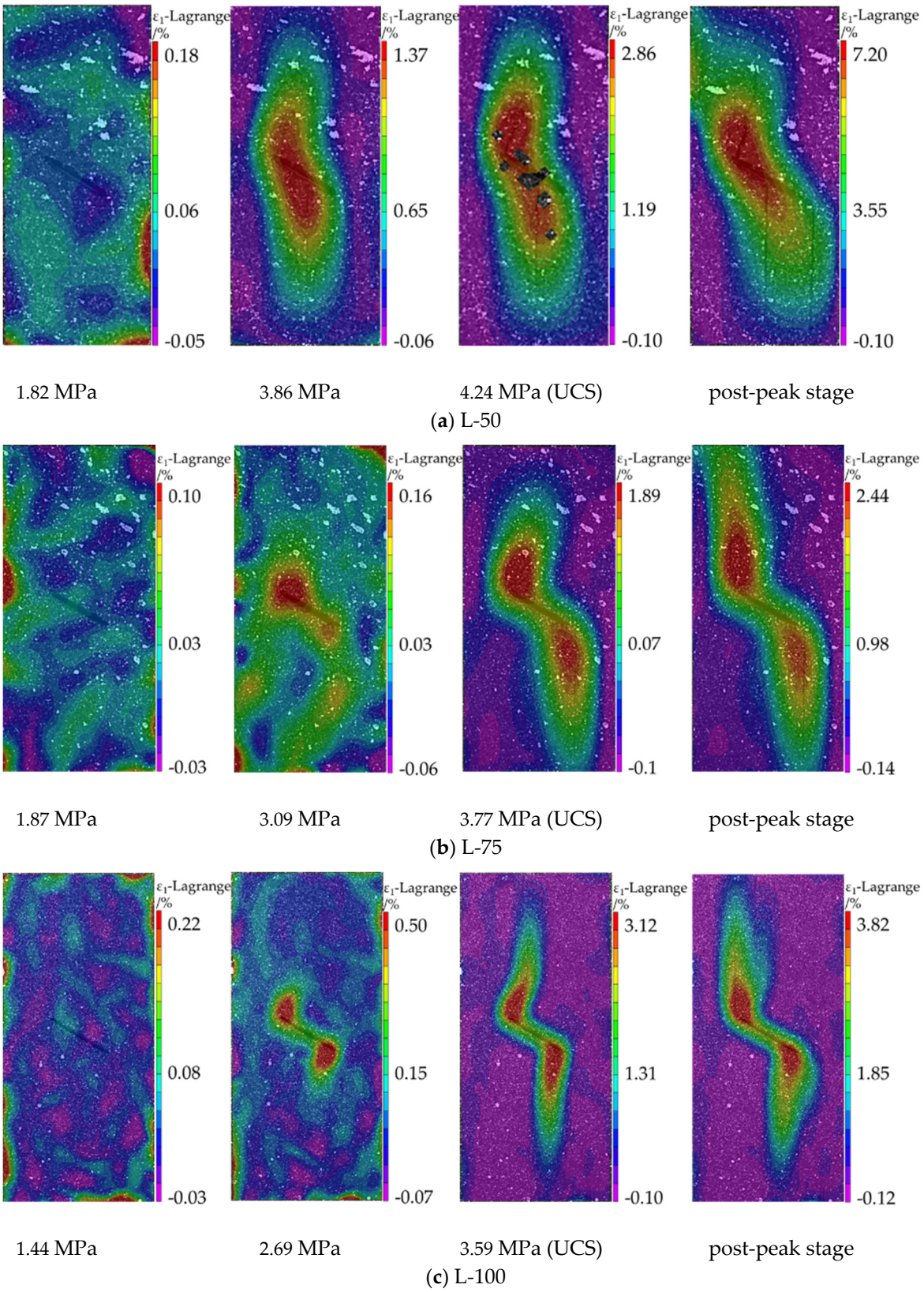

Figure 9. Evolution of the global strain field of the 30° fractured specimen.

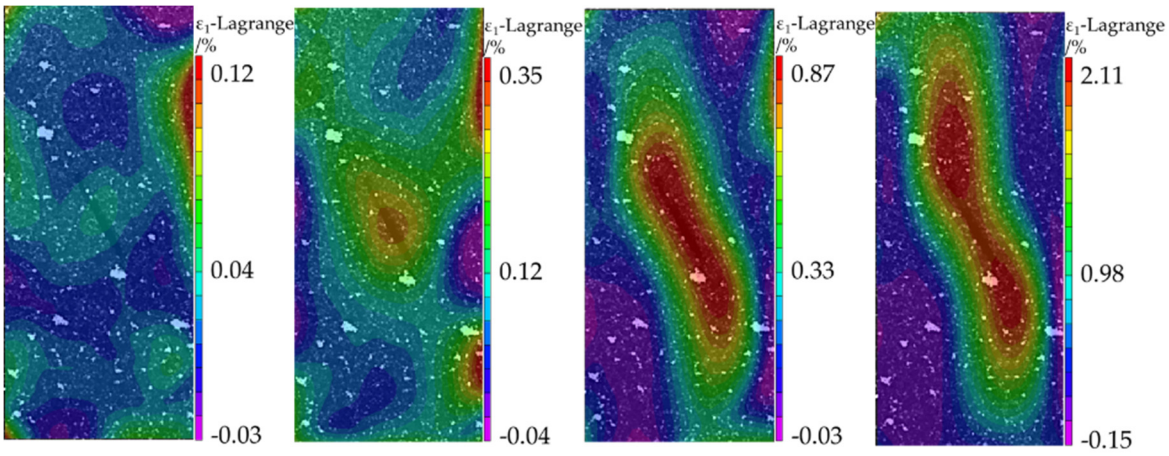

1.82 MPa 3.86 MPa 5.27 MPa (UCS) post-peak stage

(**a**) L-50

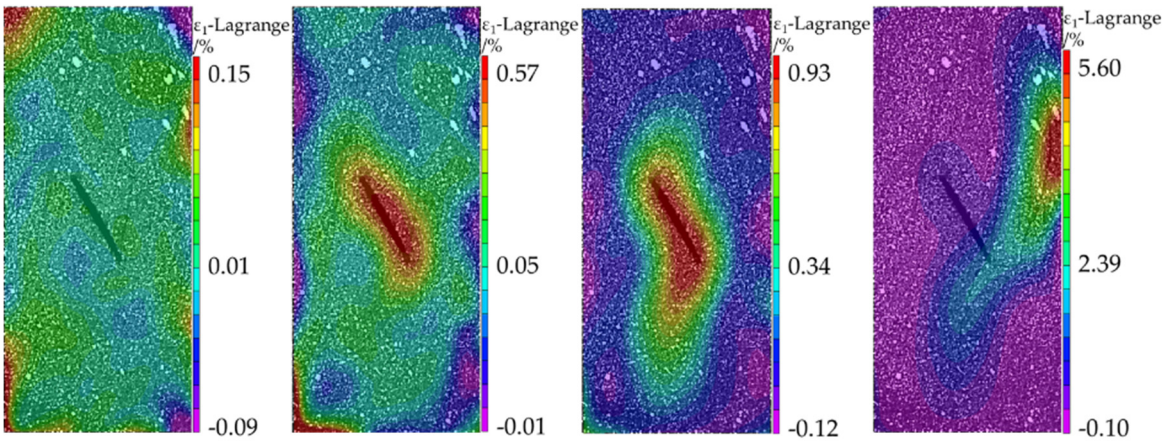

1.84 MPa 3.58 MPa 4.69 MPa (UCS) post-peak stage

(**b**) L-75

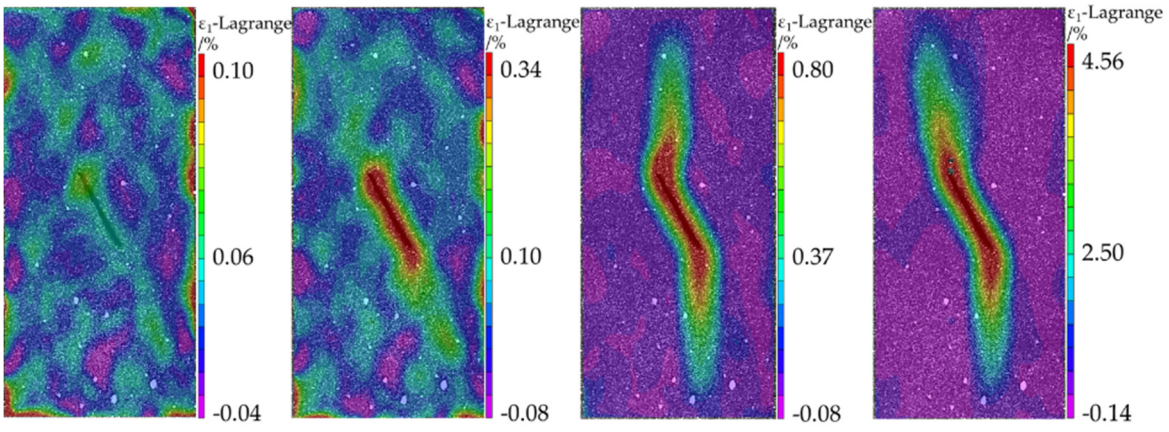

1.80 MPa 3.27 MPa 3.88 MPa (UCS) post-peak stage

(**c**) L-100

Figure 10. Evolution of the global strain field of the 60° fractured specimen.

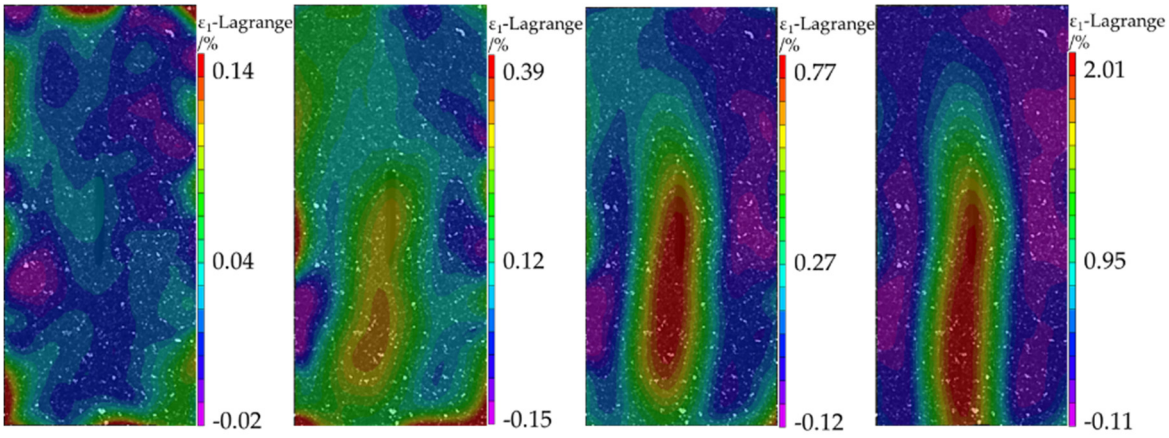

1.63 MPa 4.95 MPa 7.39 MPa (UCS) post-peak stage

(**a**) L-50

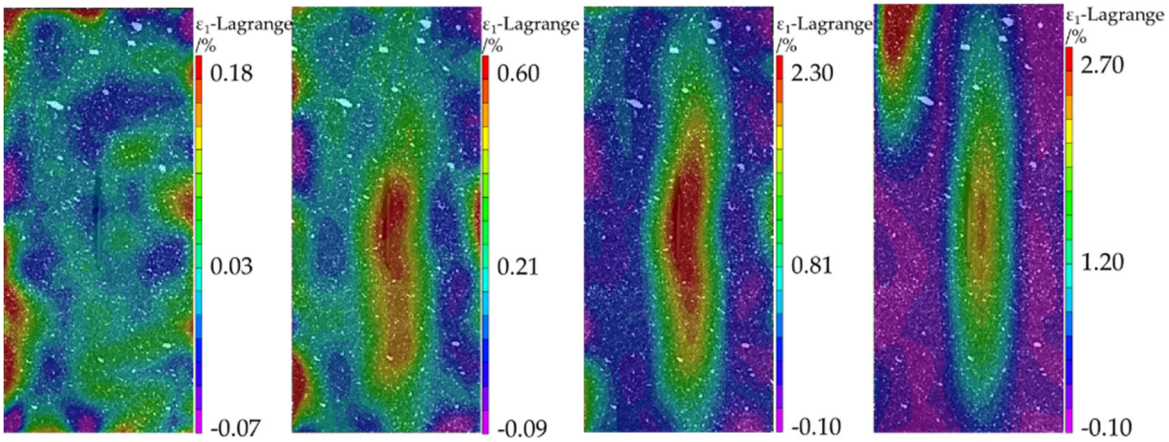

1.65 MPa 4.52 MPa 5.96 MPa (UCS) post-peak stage

(**b**) L-75

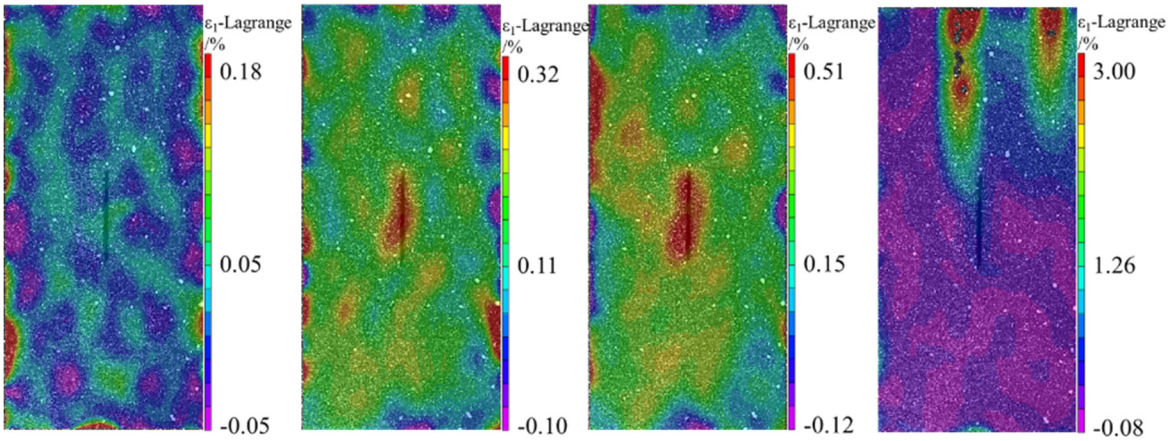

1.79 MPa 4.12 MPa 5.41 MPa (UCS) post-peak stage

(**c**) L-100

Figure 11. Evolution of the global strain field of the 90° fractured specimen.

As shown in Figure 8, The global strain evolution diagrams of each specimen in the whole loading process have an obvious propagation rule of the strain concentration

band when α is 0°. When the stress of L-50, L-75, and L-100 specimens reached 1.87 MPa, 2.18 MPa, and 2.16 MPa in the plastic deformation stage, respectively, the strain concentration zone was formed at the positions of prefabricated fracture. The strain concentration zone propagated to the upper and lower ends of the specimens as the loading went on. When loaded to the UCS, the strain concentration band is formed into both ends of the specimen. Both L-75 and L-100 specimens generated a new concentrated band on the other side of the prefabricated fracture tip, which propagated to the upper and lower ends of the specimen, respectively, and the strain concentration band of the L-50 specimen had no obvious characteristic change after post-peak brittle failure stage.

The trend of strain concentration band indicates the trend of crack initiation and propagation. The cracks of the L-50 specimen initiate in the middle of the prefabricated fracture, while the cracks of the L-75 and L-100 specimens initiated at the tip of the prefabricated fracture and propagated along the loading direction until reaching the upper and lower ends of the specimen. In summary, the crack initiation position of the 3D printing specimens shifted from the middle of the fracture to the end of the fracture with the increase of the specimen size when α is 0°. The crack propagation direction was similar to that of the rock-like specimen and extended along the loading direction [34]. It preliminarily proves the feasibility of the sand powder 3D printed specimens in rock mass mechanics.

Figures 9 and 10 depict the global strain evolution diagrams of the 30° and 60° fractured specimens at different stages on the curve. It can be seen that there is roughly the same evolution trend of the global strain field for each specimen when α is 30° and 60°; the strain concentration zone is initially formed at the fracture tips. When the 60° fractured specimen of L-75 reaches the UCS, the strain concentration zone develops towards the lower end of the specimen and finally forms a strain concentration band at a certain angle with the fracture. When other fractured specimens reach the UCS, the strain concentration zone at the tip propagates to the upper and lower ends of the specimen at the same time, forming an approximately antisymmetric strain concentration band. The propagation rule of strain concentration is consistent with previous studies [35]. It indicates that the cracks at the 60° fractured specimen of L-75 initiate at the lower end of the fracture and then propagate in the direction of a certain angle with the fracture. The cracks of other specimens initiate at the fracture tips at the same time and then develop through the whole specimen along the loading direction. The developing rule of the L-75 strain concentration band is different from other specimens When α is 60°. The analysis believes that it is caused by insufficient bonding between the binder and sand powder, which causes cracks to expand easily at the lower end of the prefabricated fracture.

Therefore, when α is 30° and 60°, the crack propagation rule of each specimen is roughly the same, which initiates from the fracture tip and propagates to the upper and lower ends of the specimen along the loading direction until it runs through the whole specimen.

Figure 11 shows the global strain evolution diagram of the 90° fractured specimen during the loading process. It has been found that the stress of L-50 and L-75 specimens reaches 4.95 MPa and 4.52 MPa at the plastic deformation stage when α is 90°, the strain concentration zone appears at the bottom of the specimen near the prefabricated fracture, then it develops upward to the top center of the specimen as the loading progresses. Compared with the previous study, the propagation rule of strain concentration is similar to some extent [34]. The developing rule of the L-100 strain concentration zone is not obvious, and the top of the specimen was damaged during loading; the analysis shows that it is also caused by insufficient bonding between the binder and sand powder, which causes crack not initiate at the fracture position, but at the specimen's end. But as is shown in Figure 11c, when the stress in the plastic deformation stage reaches 4.12 MPa, the strain concentration zone appears at the prefabricate fracture. It can be shown that when the α is 90°, cracks of all specimens initiate near the bottom of the specimen and then propagate along the loading direction, forming macroscopic cracks and leading to the failure of the specimen.

3.4. Failure Mode Analysis of Fractured Specimen

Figures 12–15 show the distribution of horizontal displacement field of 0°, 30°, 60°, and 90° fractured specimens after processing using a digital speckle system, the unit of value in the figure is the pixel. The larger the pixel value is, the greater the displacement is. The system sets horizontal right as positive and left as negative. Combined with the evolution diagram of the global strain field, it is used to analyze the failure modes of specimens of various sizes.

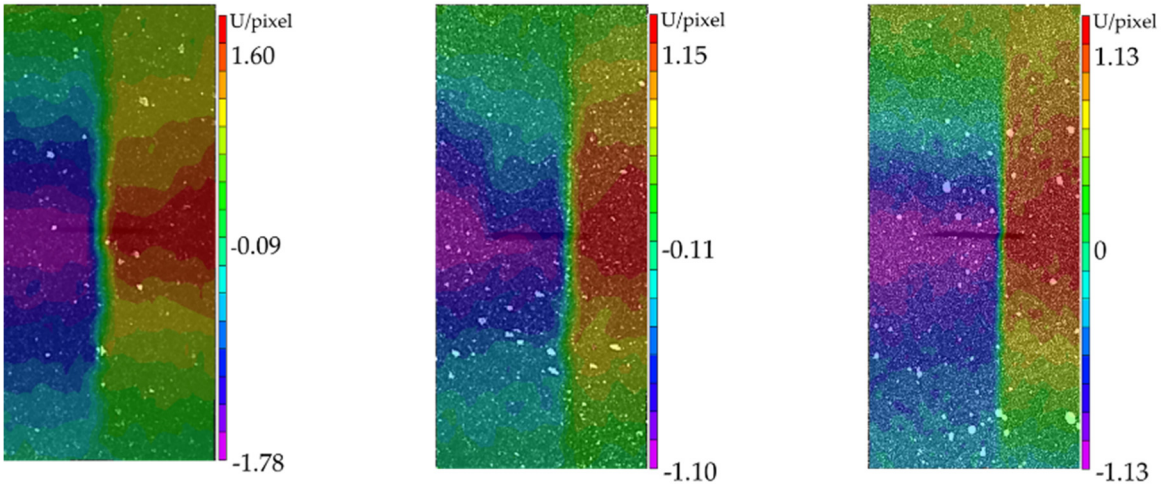

(**a**) L-50 (**b**) L-75 (**c**) L-100

Figure 12. Horizontal displacement field on the surface of 0° fractured specimen after the peak.

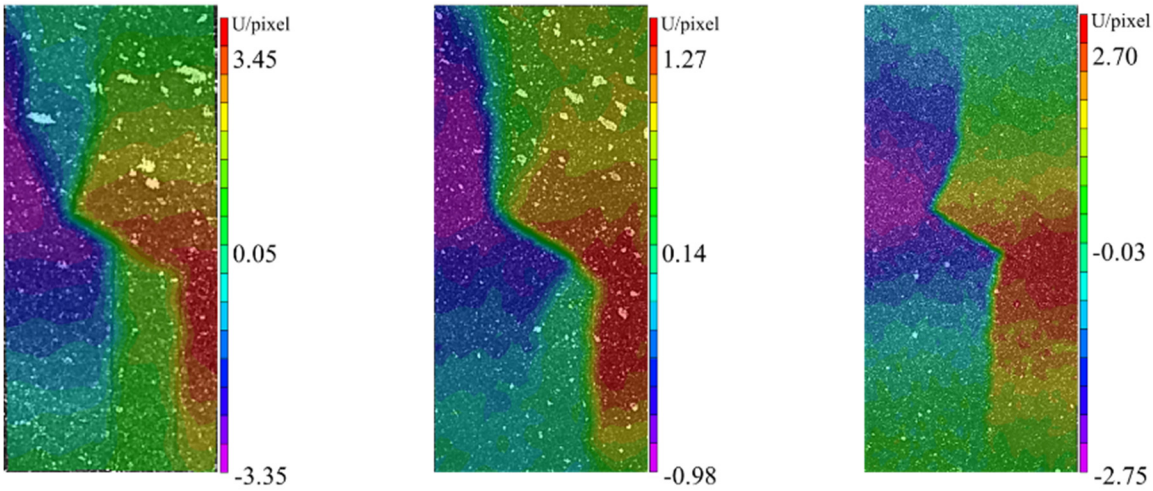

(**a**) L-50 (**b**) L-75 (**c**) L-100

Figure 13. Horizontal displacement field on the surface of 30° fractured specimen after the peak.

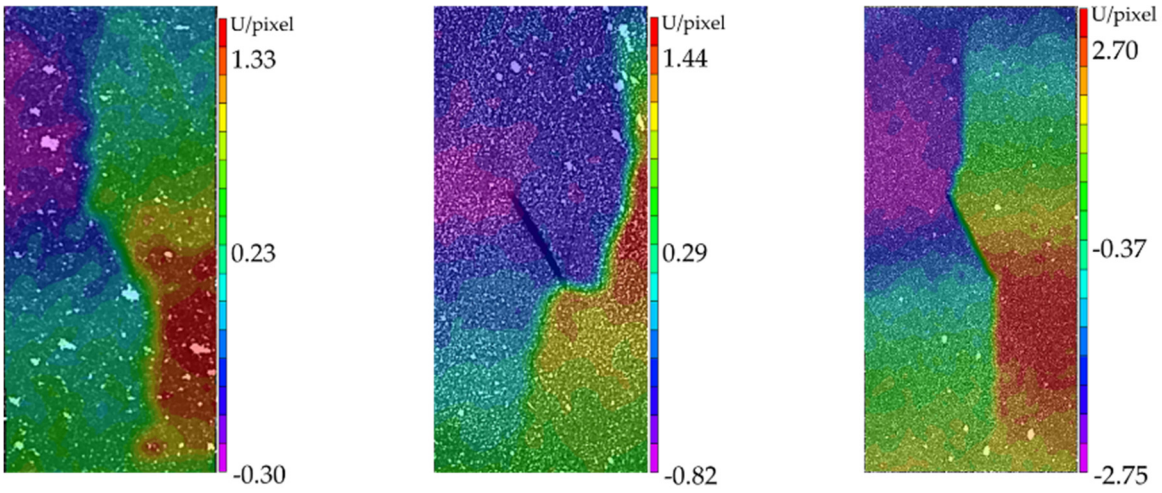

(**a**) L-50 (**b**) L-75 (**c**) L-100

Figure 14. Horizontal displacement field on the surface of 60° fractured specimen after the peak.

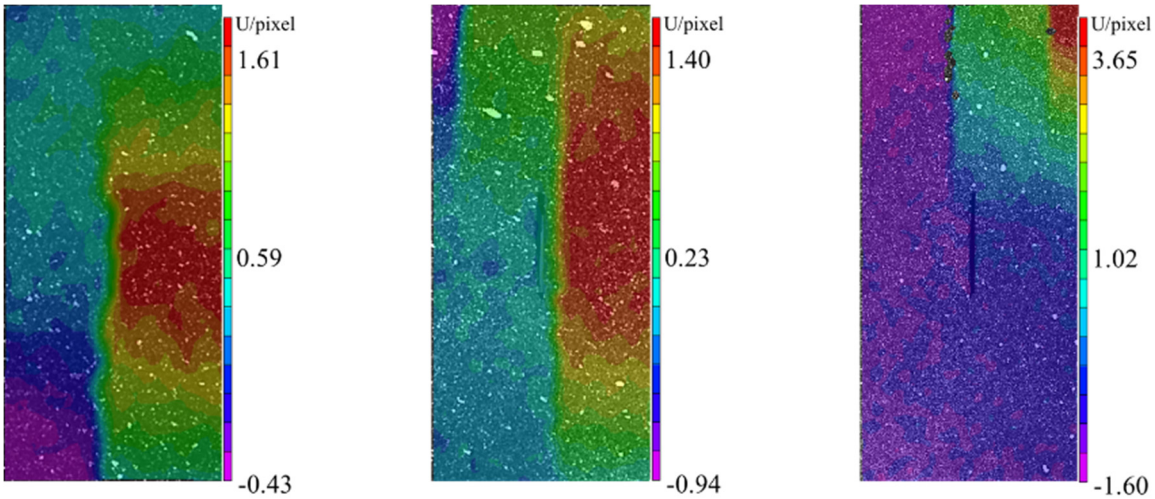

(**a**) L-50 (**b**) L-75 (**c**) L-100

Figure 15. Horizontal displacement field on the surface of 90° fractured specimen after the peak.

Through observation and analysis, it can be concluded that:

(1) When α is 0°, the maximum horizontal displacement field of each specimen is approximately symmetrically distributed on both sides of the prefabricated fracture. As is shown in Figure 12a, The maximum horizontal displacement at the fracture is −1.78 pixels and 1.60 pixels; the cracks start from the prefabricated fracture under tensile stress, and shear slip occurs in the specimen when the cracks propagate to the upper and lower ends, the tensile crack changes into a shear crack. Finally, the specimen presents a mixed failure mode of tensile and shear.

(2) When α is 30° and 60°, the maximum horizontal displacement field gradually develops from the upper and lower sides of the prefabricated fracture to the two tips and is located on the left and right sides of the prefabricated fracture in an antisymmetric distribution [34]. When α is 30°, as is shown in Figure 13a, the maximum horizontal displacement on the upper and lower sides of the fracture is −3.35 pixels and 3.45 pixels, respectively. The crack initiates by tensile stress, and then the tensile crack becomes a shear crack during the process of propagating the upper and lower ends.

Finally, the specimen presents a mixed failure mode of tensile and shear. When α is 60°, as is shown in Figure 14a,c, The crack propagation of L-50 and L-100 specimens is always affected by shear stress, and the specimens show shear failure mode. As is shown in Figure 14b, The crack of the L-75 specimen is initiated by the tensile stress and is controlled by the shear stress and the tensile stress in turn during the propagation process. Finally, the L-75 specimen shows a mixed failure mode of tension and shear.

(3) When α is 90°, the maximum horizontal displacement field regularity of each specimen is not obvious. The maximum horizontal displacement field of L-50 and L-100 specimens is located near the prefabricated fracture. As is shown in Figure 15a, the L-50 specimen horizontal displacement field at the lower end of the fracture is larger, which is −0.17 pixels in the left direction and 1.1 pixels in the right direction. The crack is initiated by shear stress. Shear slip occurs when propagating up and down, resulting in the complete loss of bearing capacity of the specimen. The L-50 specimen presents a shear failure mode. As is shown in Figure 15b, the crack initiation of the L-75 specimen is also controlled by shear stress and finally presents shear failure mode. As is shown in Figure 15c, The L-100 specimen's maximum horizontal displacement field does not appear near the prefabricated fracture but is located at the upper end of the specimen, which is −1.60 pixels and 1.35 pixels, respectively. The crack is initiated by tensile stress. The L-100 specimen finally shows tensile failure mode.

In this paper, the uniaxial compression tests and DIC technology were carried out on 3D printing fractured specimens of different sizes in order to study the size effect on the mechanical properties and failure pattern of the fractured rock mass. The conclusions are almost consistent with the size effect of complete specimens by previous studies [7,36], the UCS and Elasticity Modulus decrease with an increase in the specimen size. Under the condition of the same fracture angle, the size effect on the propagation and distribution of strain concentration and horizontal displacement field are generally consistent with previous studies [34,35].

4. Mechanism Analysis of Size Effect

There are two reasons for the rock size effect: One is the rock heterogeneity [2,5]. The rock contains microdefects such as fractures and joints. As the size increases, the degree of the microdefects contained in the interior increases, and the strength of the rock decreases accordingly. The other is the friction between the end faces of the rock specimen and the loading platens [37,38]. With the increase of the length-to-diameter ratio, the state of internal stress changes, and the strength also changes. When the length-to-diameter ratio is greater than or equal to 2.0, the rock material is not affected by the end friction effect. In this experiment, the length-to-diameter ratio was fixed at 2.0, which avoids the end constraint of the testing machine as much as possible.

The rock mass contains various levels of defects. The faults, flaws, and fractures, etc., are called high-level defects in the rock, and the microcracks and micropores, etc., are called low-level defects in the rock [39]. The corresponding research results show that high-level defects play a leading role in the strength and deformation of rock mass when defects of different sizes and levels coexist. In the process of the uniaxial test, if the specimen internal defect size is much smaller than the specimen size, it belongs to the low-level defect, which has little influence on the deformation and strength; if the specimen internal defect size is much bigger than the specimen size, it belongs to the high-level defect which has a significant influence on the deformation and strength.

Combined with the relevant size effect research [33,39], the microscopic analysis of the 3D printing specimen was carried out. The research believes that the size effect is due to the heterogeneity of materials. As shown in Figure 16, The particle shape of the 3D printing specimen is extremely irregular, the thickness of the surface binder is different, and large pores are easily generated when the particles are bonded, which affects the mechanical properties of the specimen. In small-size specimens, the probability of finding larger cracks

is small and has little effect on strength; with the increase of volume, the probability of pores joining into higher-level cracks increases in a specimen, and the influence of porosity on the specimen's strength increases. As a result, the specimen's strength decreases with the increase in size. The results and analysis of the mechanism of size effect are consistent with previous research [33,39].

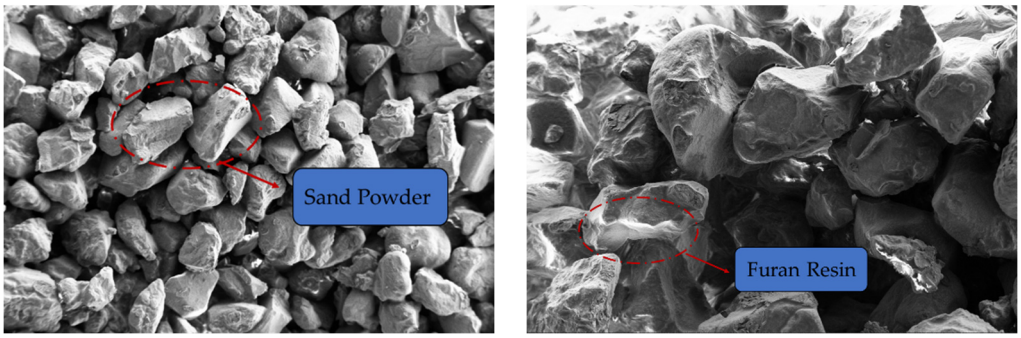

(**a**) Sand Powder microscope images (**b**) Furan Resin microscope images

Figure 16. Scanning Electron Microscope of 3D printing specimen.

When the specimen contains a prefabricated fracture, the strength of small-size specimens is affected by the prefabricated fracture. The strength of large-size specimens is controlled by prefabricated fracture and high-level cracks. Therefore, under the condition of the same fracture inclination angle, with the size increase, the size effect is more obvious, and the strength of the specimen is lower.

5. Results and Discussion

As a preliminary study, the results of this study show that sand powder 3D printing can properly simulate the mechanical behaviors of rocks and can be considered a useful method for generating rock-like specimens with fractures.

Through the research on the hot topic in the field of rock mechanics and engineering—Size Effect, it can be seen that there is a significant size effect on strength characteristics and deformation and failure characteristics of fractured specimens with different sizes based on sand powder 3D printing, the rule is basically consistent with rock size effect, the feasibility of applying sand powder 3D printing technology to study the size effect of fractured rock mass is verified. In the study of the rock size effect, it is difficult to ensure specimen homogeneity due to the difficulty of large-scale coring and the limitation of processing large-sized and fractured specimens in the production of traditional rock-like specimens. This provides an innovative test method for size effect experimental research.

The coal measure strata are affected by sedimentation, resulting in weak lithology of the surrounding rock, development of joints and fractures, and the significant size effect of a rock mass. The rock mechanics test results of complete and small-size rock specimens are difficult to be directly used to guide the stability analysis of fissure surrounding rock and the roadway support design. The sand powder 3D printing technology can produce a large number of specimens with good homogeneity, complex fracture, and different sizes. The elastoplastic mechanical properties and deformation and failure characteristics of the specimen are similar to those of the soft surrounding rocks in coal measures [22,25,40].

The sand powder 3D printing technology has broad application prospects in the field of rock mass mechanics. Compared with the complexity and difficulty of making natural rock specimens and the limitations of traditional manual specimen preparation, the application of sand powder 3D printing technology in rock mass mechanics research has become a future trend. The sand powder 3D printing technology overcomes many difficulties encountered in traditional specimen preparation based on the reduction manufacturing principle, such as difficulty in producing complex models, time-consuming and laborious specimen preparation, and large discreteness of specimen, showing unparalleled advantages.

However, the application of sand powder 3D printing technology in rock mass mechanics also has limitations, such as expensive equipment, limited model size, and limited materials for printing rock specimens. Even so, there is still reason to believe that with the continuous improvement of 3D printing technology, the decline in printing costs, and breakthroughs in material technology, its application in rock mass mechanics will be more extensive and in-depth.

6. Conclusions

In this study, sand powder specimens were based on 3D printing technology and were prepared to study the size effect through uniaxial compression tests combined with DIC technology. The strength variation rule, the crack evolution rule, and the failure mode of the specimen were studied from the perspective of the global strain evolution diagram and horizontal displacement cloud diagram, and the following conclusions were obtained:

(i) Under the condition of fracture with different inclination angles, the UCS and Elasticity Modulus of 3D printing specimens decreases with the increase of size. The influence of size effect on specimens with different fracture characteristics is different. The size effect of UCS is most obvious for the 0° fractured specimen, the 30° fractured specimen is the least obvious, and the size effect of Elasticity Modulus is most significant for the 30° and 60° fractured specimens in different size ranges.

(ii) When α is 0°, with the increase of the specimen size, the crack initiation position shifts from fracture middle to fracture end; When α is 0° and 60°, each specimen crack initiates at the fracture tip and propagates to specimen upper and lower ends after initiation; When α is 90°, each specimen fracture initiates from the bottom near the prefabricated fracture and then propagates to the specimen upper end.

(iii) When α is 0° and 30°, each specimen exhibits tensile and shear mixed failure; When α is 60°, each specimen exhibits shear failure; When α is 90°, with the increase of the specimen size, each specimen transitions from the failure of shear to the failure of tension.

(iv) Combined with the Scanning Electron Microscopy of the 3D printing specimen, the degree of bonding between the particles inside the specimen was analyzed. The size effect of fractured rock mass is closely related to the defect level inside the rock mass. The size effect originates from the heterogeneity inside the material.

According to the simulated target lithology, the printing materials and parameters can be changed so as to obtain a specimen with mechanical properties closer to the target rock. It is helpful to carry out the study of the size effect of complex fractured rock mass on the strength characteristics and failure mechanism of surrounding rock; At the same time, combined with the core CT scanning technology, the internal fracture structure of the original rock core can be obtained, then the three-dimensional digital model is reconstructed and imported into the 3D printing system which can accurately produce specimen with the same internal structure as the original rock. It is convenient to carry out various indoor tests and basic research, which has broad application prospects.

Author Contributions: Conceptualization, W.W. and L.J.; methodology, Y.Z.; software, W.W.; validation, W.W., L.J. and Y.Z.; formal analysis, J.Z.; investigation, G.L.; resources, L.J.; data curation, H.S.M.; writing—original draft preparation, W.W.; writing—review and editing, Y.Z.; visualization, L.J.; supervision, H.S.M.; project administration, L.J.; funding acquisition, L.J. All authors have read and agreed to the published version of the manuscript.

Funding: This study was financially supported by the Young Scientist Project of the National Key Research and Development Program of China (Grant No. 2021YFC2900600), the National Natural Science Foundation of China (52074166) and the Shandong Province (ZR2021YQ38), and the Open Grant of State Key Laboratory of Mining Response and Disaster Prevention and Control in Deep Coal Mines (SKLMRDPC20KF02).

Data Availability Statement: Data used to support the results of this study can be found in this manuscript text.

Conflicts of Interest: The authors declare that they have no known competing financial interests or personal relationships that could have appeared to influence the work reported in this paper.

References

1. Xie, H.P.; Chen, Z.H. *Rock Mechanics*; Beijing Science Press: Beijing, China, 2004.
2. Weibull, W.; Rockey, K.C. Fatigue Testing and Analysis of Results. *J. Appl. Mech.* **1961**, *29*, 607. [CrossRef]
3. Hudson, J.A.; Crouch, S.L.; Fairhurst, C. Soft, stiff and servo-controlled testing machines: A review with reference to rock failure. *Eng. Geol.* **1972**, *6*, 155–189. [CrossRef]
4. Darbor, M.; Faramarzi, L.; Sharifzadeh, M. Size-dependent compressive strength properties of hard rocks and rock-like cementitious brittle materials. *Geosystem Eng.* **2018**, *22*, 179–192. [CrossRef]
5. Weibull, W. A Statistical Theory of Strength of Materials. *IVB-Handl* **1939**, *151*, 1034.
6. Bazant, Z.P. Size Effect in Blunt Fracture: Concrete, Rock, Metal. *J. Eng. Mech.* **1984**, *110*, 518–535.
7. Li, K.; Yin, Z.Y.; Han, D.; Fan, X.; Cao, R.; Lin, H. Size Effect and Anisotropy in a Transversely Isotropic Rock Under Compressive Conditions. *Rock Mech. Rock Eng.* **2021**, *54*, 4639–4662. [CrossRef]
8. Zhai, H.; Masoumi, H.; Zoorabadi, M.; Canbulat, I. Size-dependent Behaviour of Weak Intact Rocks. *Rock Mech. Rock Eng.* **2020**, *53*, 3563–3587. [CrossRef]
9. Faramarzi, L.; Rezaee, H. Testing the effects of sample and grain sizes on mechanical properties of concrete. *J. Mater. Civ. Eng.* **2018**, *30*, 04018065. [CrossRef]
10. Tuncay, E.; Özcan, N.T.; Kalender, A. An approach to predict the length-to-diameter ratio of a rock core specimen for uniaxial compression tests. *Bull. Eng. Geol. Environ.* **2019**, *78*, 5467–5482. [CrossRef]
11. Pappalardo, G.; Mineo, S.; Marchese, G. Effects of cubical specimen sizing on the uniaxial compressive strength of etna volcanic rocks (Italy). *Ital. J. Eng. Geol. Environ.* **2013**, *2*, 45–54.
12. Xue, D.; Zhou, J.; Liu, Y.; Gao, L. On the excavation-induced stress drop in damaged coal considering a coupled yield and failure criterion. *Int. J. Coal Sci. Technol.* **2020**, *7*, 58–67. [CrossRef]
13. Wang, J.; Yang, J.; Wu, F.; Hu, T.; Faisal, S.A. Analysis of fracture mechanism for surrounding rock hole based on water-filled blasting. *Int. J. Coal Sci. Technol.* **2020**, *7*, 704–713. [CrossRef]
14. Chen, D.; Chen, H.; Zhang, W.; Lou, J.; Shan, B. An analytical solution of equivalent elastic modulus considering confining stress and its variables sensitivity analysis for fractured rock masses. *J. Rock Mech. Geotech. Eng.* **2022**, *14*, 825–836. [CrossRef]
15. Li, G.; Hu, Y.; Tian, S.M.; Huang, H.L. Analysis of deformation control mechanism of prestressed anchor on jointed soft rock in large cross-section tunnel. *Bull. Eng. Geol. Environ.* **2021**, *80*, 9089–9103. [CrossRef]
16. Darlington, W.J.; Ranjith, P.G.; Choi, S.K. The Effect of Specimen Size on Strength and Other Properties in Laboratory Testing of Rock and Rock-Like Cementitious Brittle Materials. *Rock Mech. Rock Eng.* **2011**, *44*, 513. [CrossRef]
17. Bahrani, N.; Kaiser, P.K. Numerical investigation of the influence of specimen size on the unconfined strength of defected rocks. *Comput. Geotech.* **2016**, *77*, 56–67. [CrossRef]
18. Stavrou, A.; Murphy, W. Quantifying the effects of scale and heterogeneity on the confined strength of micro-defected rocks. *Int. J. Rock Mech. Min. Sci.* **2018**, *102*, 131–143. [CrossRef]
19. Ju, Y.; Xie, H.; Zheng, Z.; Lu, J.; Mao, L.; Gao, F.; Peng, R. Visualization of the complex structure and stress field inside rock by means of 3D printing technology. *Chin. Sci. Bull.* **2014**, *59*, 5354–5365. [CrossRef]
20. Jiang, Q.; Liu, X.; Yan, F.; Yang, Y.; Xu, D.; Feng, G. Failure Performance of 3DP Physical Twin-Tunnel Model and Corresponding Safety Factor Evaluation. *Rock Mech. Rock Eng.* **2020**, *54*, 109–128. [CrossRef]
21. Kong, L.; Ostadhassan, M.; Li, C.; Tamimi, N. Can 3D Printed Gypsum Samples Replicate Natural Rocks? An Experimental Study. *Rock Mech. Rock Eng.* **2018**, *51*, 3061–3074. [CrossRef]
22. Tian, W.; Han, N.V. Mechanical properties of rock specimens containing prexisting flaws with 3d printed materials. *Strain* **2017**, *53*, e12240. [CrossRef]
23. Gomez, J.S.; Chalaturnyk, R.J.; Zambrano-Narvaez, G. Experimental Investigation of the Mechanical Behavior and Permeability of 3D Printed Sandstone Analogues Under Triaxial Conditions. *Transp. Porous Media* **2019**, *129*, 541–557. [CrossRef]
24. Xu, Q.; Jiang, L.S. Effect of layer thickness on the physical and mechanical properties of sand powder 3d printing specimens. *Front. Earth Sci.* **2021**, *2021*, 1112. [CrossRef]
25. Jiang, L.S.; Wu, X.Y.; Wang, Q.W. Study on dynamic mechanical behaviors of sand-powder 3D printing rock-like specimens under coupled static and dynamic loads. *J. China Coal Soc.* **2022**, *47*, 1196–1207.
26. He, M.C.; Jing, J.H.; Sun, X.M. *Soft Rock Engineering Mechanics*; Beijing Science Press: Beijing, China, 2020.
27. Liu, P.; Ju, Y.; Ranjith, P.G.; Zheng, Z.; Wang, L.; Wanniarachchi, A. Visual representation and characterization of three-dimensional hydrofracturing cracks within heterogeneous rock through 3D printing and transparent models. *Int. J. Coal Sci. Technol.* **2016**, *3*, 284–294. [CrossRef]
28. Mazhar, H.; Osswald, T.; Negrut, D. On the use of computational multi-body dynamics analysis in SLS-based 3D printing. *Addit. Manuf.* **2016**, *12*, 291–295. [CrossRef]
29. Gao, Y.T.; Wu, T.H.; Zhou, Y. Application and prospective of 3D printing in rock mechanics: A review. *Int. J. Miner. Metall. Mater.* **2021**, *28*, 17. [CrossRef]

30. Pei, Z.R. A Study on Mechanical Characteristics of Flawed Rock Mass Specimens Based on CT Scanning and 3D Printing Technology. Master's Thesis, Chang'an University, Xi'an, China, 2018.
31. Zhao, G.F.; Liu, L.Z.; Chen, L.W. *Regulation for Testing the Physical and Mechanical Properties of Rock*, 18th ed.; Ministry of Land and Resources of the People's Republic of China: Beijing, China, 2015.
32. Mei, Y.X.; Zhao, G.F.; Zeng, J. *Regulation for Testing the Physical and Mechanical Properties of Rock*, 19th ed.; Ministry of Land and Resources of the People's Republic of China: Beijing, China, 2015.
33. Wu, F.Q.; Qiao, L.; Guan, S.G.; Zhang, Q.T.; Wang, Z.Y.; Wu, J. Study on size effect of uniaxial compression tests of small size rock samples. *Chin. J. Rock Mech. Eng.* **2021**, *40*, 865–873.
34. Ai-Bing, J.; Shu-Liang, W.; Ben-Xin, W.; Hao, S.; Yi-Qing, Z. Study on the fracture mechanism of 3D-printed-joint specimens based on DIC technology. *Rock Soil Mech.* **2020**, *41*, 3214–3224.
35. Zhao, C.; Liu, F.; Tian, J. Study on single crack propagation and damage evolution mechanism of rock-like materials under uniaxial compression. *Chin. J. Rock Mech. Eng.* **2016**, *35* (Suppl. S2), 3626–3632.
36. Quiñones, J.; Arzúa, J.; Alejano, L.R.; García-Bastante, F.; Mas Ivars, D.; Walton, G. Analysis of size effects on the geomechanical parameters of intact granite samples under unconfined conditions. *Acta Geotech.* **2017**, *12*, 1229–1242. [CrossRef]
37. Mogi, K. *Experimental Rock Mechanics*; Taylor and Francis: London, UK, 2007; pp. 12–14, 36–37, 83–110.
38. Wawersik, W.R. *Detailed Analysis of Rock Failure in Laboratory Compression Tests*; University of Minnesota: Minneapolis, MN, USA, 1968.
39. Feng, Z.C.; Zhao, Y.S. Control effect of fissure scale on deformation and failure of rock mass. *Chin. J. Rock Mech. Eng.* **2008**, *27*, 78–83.
40. Gell, E.M.; Walley, S.M.; Braithwaite, C.H. Review of the Validity of the Use of Artificial Specimens for Characterizing the Mechanical Properties of Rocks. *Rock Mech. Rock Eng.* **2019**, *52*, 2949–2961. [CrossRef]